International Journal of Heat and Mass Transfer 52 (2009) 2498–2506

Contents lists available at ScienceDirect

International Journal of Heat and Mass Transfer

journal homepage: www.elsevier.com/locate/ijhmt

Impingement of an impact jet onto a spherical cavity. Flow structure and heat transfer

V.I. Terekhov *, S.V. Kalinina, Yu.M. Mshvidobadze, K.A. Sharov

Kutateladze Institute of Thermophysics SB RAS, Novosibirsk, Russia

ARTICLE INFO

Article history:
Received 12 January 2009
Available online 9 March 2009

Keywords:
Impact jet
Heat transfer
Spherical cavity
Heat-flow pulsations

ABSTRACT

An experimental study of flow characteristics and heat transfer for jet impingement cooling of obstacles in the form of single spherical cavities is reported. The distributions of flow velocities between the nozzle and the obstacle, and also the fields of pressure and heat-transfer coefficients inside the cavity were measured. It is found that, at a value of depth the cavity generates the large-scale toroidal vortex, essentially influencing on the heat transfer. The cavity flow becomes unstable, exhibiting low-frequency pulsations of local heat fluxes. In the examined ranges of Reynolds numbers, $Re = (1.2–5.8)10^4$, and cavity depths (equal to or smaller than $0.5D_c$) the local heat-transfer intensity in the cavity is lower than that on a flat obstacle; yet, this reduction is almost fully compensated by increased area of the heat-exchanging surface.

1. Introduction

Heat-exchanging surface geometry modification is believed to be an effective means to control heat transfer during jet impingement cooling of surfaces. Indeed, as it was shown in [1–3], heat flows from a body streamlined with an impinging jet, especially those in the vicinity of the stagnant point, are defined by radial gradients of pressure, in turn largely defined by the body shape. Yet, such relatively a simple situation is not always the case. For instance, as a result of vortex formation processes in local flow detachment zones at obstacles in the form of cavities/trenches a complex unstable flow structure can emerge exhibiting large-scale low-frequency flow pulsations, the Coanda effect, etc. [4]. Under such conditions, adequate prediction of heat-transfer processes remains problematic.

In the present study, we examined the flow structure and heat transfer during impingement cooling of an obstacle in the form of spherical cavity with an axisymmetric jet flow. Such configurations attract considerable attention since these configurations, streamlined by flows, proved to be efficient generators of unusual pulsating flow regimes and efficient heat-transfer intensifiers [5–8]. Also, surfaces modified with cavities proved to be efficient ones in cooling internal flow paths of gas-turbine blades with a system of impact jets [9–12].

In recent years, much attention has been paid to the formation processes and stability of large-scale vortices (coherent structures), and also to the role of these vortices in heat- and mass-transfer processes proceeding in impact jet flows [13–14]. The organized structures in the jet, characterized by certain spatial and time scales bring an outlook for the control of heat transfer from a streamlined obstacle. According to analysis of available publications, in particular [15], this control is possible by a external periodic pressure perturbation, corresponding to intrinsic frequencies (time scales) of the jet, or by means of a change in the jet scale (e.g., nozzle diameter). The scope of research in the present study included the examination of flow for various obstacle shapes, when one more scale factor (cavity diameter) appears in the system.

Reported studies of impact jet flows impinging on curvilinear obstacles are few in number [16–28].

Koh and Hartnett [16] measured the distributions of pressure and time-average heat-transfer coefficients in a uniform airflow impinging on a concave hemisphere. The Reynolds number based on the hemisphere diameter D_c was varied in the range $Re_D = 6 \times 10^3$–9×10^4. The tests showed that the local heat transfer, minimal at the stagnation point, increased strongly toward the cavity edges.

Carefully visualization studies of the flow structure and measurements of recovery and heat-transfer coefficients were reported in [17–19], where an axisymmetric jet flow impinging on convex or concave a surface was examined. The temperature recovery coefficient varied in a broad range, from 0.75 to 1.2, depending on the distance from the surface, and also on the surface shape. At all other conditions being identical, the mean heat transfer from the convex surface was found to be 20–50% increased compared with the concave surface.

A scaling analysis of heat transfer for a system of impact axisymmetric jets impinging onto a concave cylindrical surface was reported in [20].

* Corresponding author.
E-mail address: terekhov@itp.nsc.ru (V.I. Terekhov).

0017-9310/$ - see front matter © 2009 Elsevier Ltd. All rights reserved.
doi:10.1016/j.ijheatmasstransfer.2009.01.018

Nomenclature

C_p	coefficient of the pressure
d_0, D_c	nozzle and cavity diameters, m
L, S	nozzle-to-surface distances, m
$Nu_0 = \alpha_0 \cdot d_0/\lambda$	stagnation point Nusselt number
$Nu_m = \alpha_m \cdot d_0/\lambda$	Nusselt number averaged over the cavity surface
Pr	Prandtl number
P_a, P_i	atmospheric pressure and pressure at the current point on the obstacle surface, Pa
q	heat-flux density, W/m^2
r, y	coordinates of the point, m
$Re = U_0 \cdot d_0/\nu$, $Re_D = U_0 \cdot D_c/\nu$	Reynolds numbers
t	time, s
T_0, T_w	temperature of the nozzle exit flow and wall, K
$Tu = (\sqrt{\overline{V_y'^2}}/U_0) \times 100\%$	turbulence intensity,%
U_0	flow velocity at the nozzle exit, m/s

Greek symbols

α	heat-transfer coefficient, W/m^2 K
λ	heat conductivity, W/mK
Δ	cavity depth, m
ν	air kinematic viscosity, m^2/s
ρ	density of air flow, kg/m^3

Subscripts

a	ambient
c	refer to the cavity
ed	refer to the vortex passage
i	refer to the current point
m	averaged over the cavity surface
max	refer to maximum
0	at the nozzle exit
w	at the obstacle surface

Chan et al. [21] examined the turbulent structure of a plane jet impinging on a convex semi-cylinder that lied on a flat surface. Measurements showed that the profiles of mean flow velocity in the wall jet were self-similar with respect to the nozzle-to-cylinder distance, whereas the intensity of velocity pulsations was shown to grow with this parameter. Numerical and experimental studies of plane jets impinging on a cylinder showed the heat-transfer intensity at the stagnation point to be higher than on the flat surface [22,23].

Heat-transfer studies of turbulent axisymmetric jets impinging on a hemisphere were reported in [24–26]. In [25,26] the diameter ratio between the hemisphere and the nozzle was varied in the range $D_c/d_0 = 11.2–29.4$. A similar geometry was used in [27] in studying the interaction of an impact jet with a hemispherical cavity. In the range of nozzle-to-obstacle distances $2 < L/d_0 < 8$ the heat transfer at the stagnation point proved to be weakly dependent on this parameter, varying in proportion to $L/d_0^{0.09}$, whereas at larger distances a stronger dependence was observed ($L/d_0^{-0.55}$). The rate of heat transfer both at the stagnation point and over the whole curved surface was found to be 15–20% greater than on the flat surface at identical flow conditions. The local distributions of heat-transfer coefficients measured in [25] at various Reynolds numbers did not admit generalization with a single dependence. In the region adjacent to the stagnation point, $0 < r/d_0 < 1.5$, the local Nusselt number followed the dependence $Nu \sim Re^{0.45–0.53}$, whereas later, as the jet spread over the surface, the correlation dependence transformed into $Nu \sim Re^{0.65–0.67}$. The power exponent in these dependences increased with increasing nozzle-to-obstacle distance.

Experimental works most close to the present study were reported in [27,28]. In paper [28] a hemispherical cavity was approached by an air flow in the direction along the vertical axis of the cavity. The jet diameter at the nozzle exit was much smaller than the cavity diameter, $D_c/d_0 = 16–50$. According to obtained data, the heat transfer at the stagnation point at fixed Reynolds number depended on the nozzle-to-obstacle distance. As compared to the case of a flat surface, the rate of heat transfer in a spherical cavity with $D_c/d_0 = 16$ was reduced. At larger diameter ratios, $D_c/d_0 = 50$, the heat transfer at the stagnation point became more intense than on the flat obstacle, and the power exponent in the Nusselt versus Reynolds number dependence increased from $n = 0.5$ for the flat obstacle to a value of $n = 0.66$ for hemisphere.

Lee et al. [27] examined the local heat transfer in a hemispherical cavity upon variation of the cavity-to-nozzle diameter ratio in the range $D_c/d_0 = 11–30$. In contrast to data obtained in [28], the rate of heat transfer was found to decrease with increasing nozzle diameter throughout the whole tested range of Reynolds number ($1 \times 10^4–5 \times 10^4$).

Thus, not only few in number are data obtained in reported studies of jet flows impinging on curvilinear obstacles; these data are also contradictory.

In the present study, being a continuation of our previous test cycle reported in [29,30] we examined the interaction between a jet and a spherical cavity. A specific feature distinguishing the present study from the studies reported in [27,28] is relatively small cavity-to-nozzle diameter ratio ($D_c/d_0 = 5.2$) typical of jet impingement cooling of dimple modified surfaces. Preliminary tests performed on a flat obstacle have allowed us to obtain well-documented data concerning the effect of surface geometry on the flow structure and heat transfer. The experiments included soot-oil visualization of surface streamlines, examination of pressure distributions over the cavity surface, measurement of flow velocity fields with the help of a digital particle image velocimetry (PIV), and also study of local heat transfer from the streamlined surface. The time-average and pulsating local heat fluxes were measured with miniaturized gradient-type heat-flux meters [31]. The varied parameters in the experiments were the Reynolds number, the nozzle-to-obstacle distance, and also the cavity depth.

2. Experimental setup and procedure

The experiments were carried out on a setup schematically depicted in Fig. 1. The jet flow issued from a subsonic nozzle with $d_0 = 8.9$ mm. The nozzle-flow contraction ratio was about 8, and the nozzle geometry was smooth, making the flow velocity at the exit plane of the nozzle quite uniform, with the turbulence intensity $Tu \cong 0.3\%$. The flow velocity at the nozzle exit U_0 was varied from 15 to 100 m/s, the corresponding Reynolds number being $Re = U_0 \cdot d_0/\nu = 10^4–6 \times 10^4$. The jet impinged onto the obstacle perpendicularly. The nozzle-to-obstacle distance S was varied from 0 to $10d_0$ with a step of $2d_0$. At $S/d_0 = 0$ the nozzle is located up to the level of a flat part of the obstacle surface. The temperature of the air flow in all experiments was close to room temperature.

The experimental conditions described in the Table 1.

At the first stage of the study, fields of pressure and flow velocity were visualized and measured. In the experiments, the obstacle was a 70 mm diameter plexiglass disc with a spherical cavity prepared at the center. The cavity diameter was $D_c = 46$ mm, whereas the cavity depth was a variable parameter, equal to $\Delta = 6$, 12 and 23 mm ($\Delta/D_c = 0.12$, 0.26 and 0.5). Holes 0.5 mm in diameter were

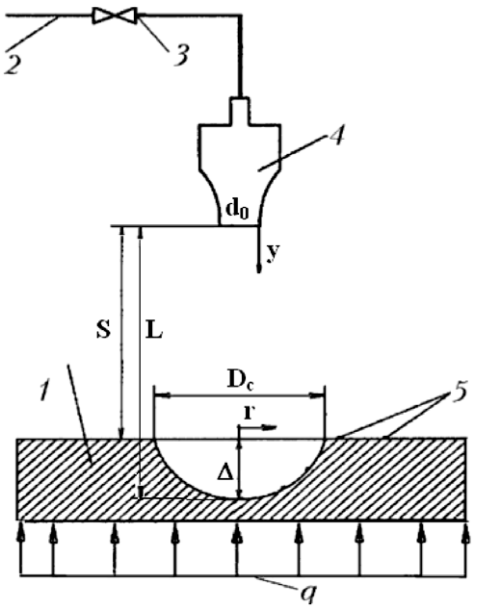

Fig. 1. Experimental setup (schematically). 1 – obstacle; 2 – air line; 3 – regulating valve; 4 – nozzle; 5 – heat-flow meters.

Table 1
Experimental conditions

No.	Δ, mm	Δ/D_c	S/d_0	Re	Measured parameters
1	0; 6; 23.	0–0.5	0–10	10^4–3×10^4	Distributions of pressure; soot-oil visualization
2	0; 6; 12; 23.	0–0.5	0–2	10^4–3×10^4	PIV-experiments
3	0	0	0–10	1.2×10^4–5.9×10^4	Heat transfer on a flat obstacle
4	12	0.26	2; 6	1.2×10^4–5.9×10^4	Heat transfer in a cavity
5	23	0.5	0–10	1.2×10^4–5.9×10^4	Heat transfer in a semispherical cavity

radially drilled in the obstacle normally to its curved surface to serve pressure taps.

The pressure was measured by the inclined micromanometers with an error of 2–3 Pa. The pressure coefficient was calculated by formula

$$C_p = 2(P_i - P_a)/\rho_0 U_0^2,$$

where $(P_i - P_a)$ is difference of pressures at a given point of the obstacle surface and in the atmosphere.

In soot-oil visualization tests, a smooth self-adhesive film was glued onto the obstacle surface. A mixture of lamp oil with offset ink was applied onto the film. Each experiment lasted for 1–1.5 min. During this time, under the action of the jet flow the working mixture poured onto the obstacle spread over its surface forming a stable picture of streamlines.

The PIV method was used to measure the fields of flow velocity in the region between the nozzle and the obstacle. The PIV system included two 50-mJ solid-state YAGNd^{3+} lasers operating in a pulsed mode at the wavelength 532.05 nm, the pulse width being 5 ns. The digital cameras had 1000×1200 pixel matrices with high photosensitivity. The measuring facility comprised a pulse synchronizer and an analog-to-digital converter, and was equipped with a computerized data acquisition and processing system. The flow was seeded with tracers with the help of an aerosol generator. The tracers were 50% water-glycerin microparticles loaded with milk powder.

Heat transfer was studied at a flat obstacle and obstacles with cavities of depths $0.26D_c$ and $0.5D_c$, and the main object was an obstacle with a semispherical cavity with maximal changes in the dynamic pattern of the flow. For these experiments the obstacle of 0.19 m diameter and 50 mm thickness was made of copper. The required temperature drop between the jet and obstacle, which in most experiments equals 313 K, was reached by means of an electric heater under the obstacle. The choice of highly heat-conductive copper as a material provided satisfaction of $T_w \cong$ const boundary condition on the obstacle. The temperatures of the streamlined wall and the flow were measured differentially by the chromel–coppel thermocouples. The local heat fluxes were measured by up to 8 gradient heat flux sensors, glued on the obstacle [31]. The characteristics of these sensors were as follow sensitivity of 10–20 mV/W, plane size of not higher than 2.5×2.5 mm (what is significantly lower than the typical sizes of the studied flow), thickness of $\approx$0.2 mm. The signals from thermocouples and sensors through a specially developed multichannel module were amplified and sent to a PC for the following calculations. Arrays of local instantaneous values of the heat flux densities were obtained in experimental, and these arrays were used for calculations of time-average local heat fluxes q_i und their pulsations. The number of values in the array was $\sim 10^4$ at the measurement time of 10–90 s. Local heat transfer coefficients α_i were determined by local heat flux densities q_i, reduced by a value of the heat flux via free convection and radiant heat transfer Δq_i, and temperature difference between the obstacle and air in the jet mouth

$$\alpha_i = (q_i - \Delta q_i)/(T_w - T_0).$$

Error Δq_i was determined experimentally by measurements of heat transfer on the model without a jet flow; in experimental this value did not exceed 5–7% of the heat flux density at the frontal point. According to the analysis and data [31], the error of measurements of the heat flux density was within 0.3–10%, for the intensity of mean square pulsations the heat fluxes changed from 4% to 50%.

3. Experimental results and discussion

3.1. Soot-oil visualization data

Experiments have shown, that the picture of lines of a current at a surface of a barrier depends on all varied parameters – Reynolds's numbers, distances between nozzle and a barrier, depths cavity. This conclusion is shown with the data of Fig. 2 where the picture is shown soot – to the oil visualization, received in dimples with different depth at Reynolds's numbers $Re = 2.8 \times 10^4$ for conditions when the barrier settled down on an initial region of a jet.

At a flat obstacle (Fig. 2a) the flow is seen to exhibit three characteristic regions, namely a central region ($2r/D_c \leqslant 0.12$) in which the jet flow impinged onto the wall and the jet made a sharp turn with the formation of Taylor–Gőrtler vortices; an annular region ($0.12 \leqslant 2r/D_c \leqslant 0.46$) in which, according to [1,3], a laminar (accelerated) boundary layer developed; and the remaining surface ($2r/D_c > 0.46$) with the flow over it becoming turbulent. A similar picture for a flat surface was reported in [1].

The flow pattern in cavities, although roughly resembling the flow pattern observed in the case of flat surfaces, had distinct specific features. The differences were manifested most brightly in the deepest, hemispherical cavity. According to Fig. 2c, in the deep cavity considerable expansion of the central flow region, from $0.12D_c$ to $0.27D_c$, was observed, with the remaining flow being more structured. The flow divided into individual vortices in the region where the flow made the 90° turn owing to the formation of Taylor–Gőrtler vortices in the vicinity of the stagnation point. At the exit from the cavity, in the region $2r/D_c = 0.9$–1.0 (the dark narrow ring in the photograph) there developed a stagnant zone.

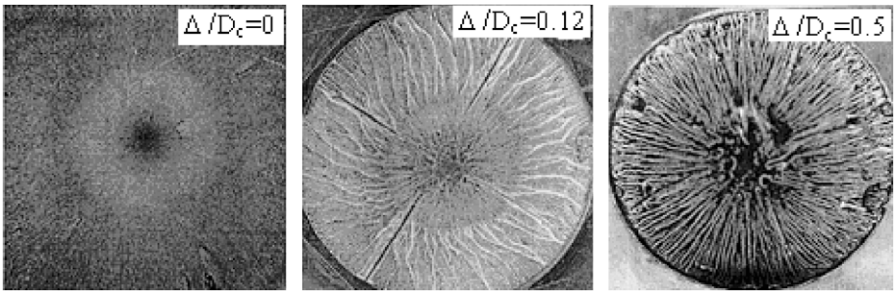

Fig. 2. Soot-oil visualization pictures. $Re = 2.8 \times 10^4$, $S/d_0 = 2$.

With obstacles installed outside the initial length of the jet flow (5–6 nozzle diameters), as well as at an increase in the flow velocity ($Re \geqslant 2.8 \times 10^4$) the soot-oil spreading picture on the obstacle surface was indefinite, exhibiting no clearly manifested flow regions.

It should be noted that Taylor–Gőrtler vortices (most authors connect these vortices with the features of jet heat transfer at a curvilinear obstacle) were observed only in a limited range of parameters.

3.2. PIV data

The primary goal of the given cycle of visualization and measurements has consisted in studying all field of current which is formed between nozzle and the obstacle. The obstacle settled down on an initial region of a jet where effects of interaction of a jet with a wall can be shown especially strongly. Reynolds's number made 1.2×10^4 and 2.8×10^4. The basic varied parameter was depth of a cavity (see the table).

The PIV measurements and visualization tests have revealed a fundamental difference between the flow patterns observed for the flat surface and the cavity. With a flat obstacle, the flow was found to make a 90° turn in the vicinity of the stagnation point, and then spread uniformly over the surface. The measurements of the velocities revealed the presence of small-size flow separation regions in the vicinity of the stagnation point.

In the case of a shallow cavity with $\Delta/D_c = 0.12$ the flow pattern was found to qualitatively resemble the flow pattern on the flat obstacle.

In the case of cavities with $\Delta/D_c = 0.26$ and 0.5 the flow made a 180° turn in the cavity and left the cavity in the direction opposite to the impact jet flow. This annular counter-flow, leaving the cavity in the peripheral regions of the cavity, was strongly unstable, displaying large-scale flow pulsations and interacting with the initial jet flow. In the region outside the cavity the flow never reattaches to the obstacle surface.

The field of mean flow velocities obtained by statistical treatment of the arrays of instantaneous flow fields revealed for dimples with depth $\Delta/D_c = 0.26$ and 0.5 a flow structure in the form of a large toroidal vortex bound up with the cavity (see Fig. 3). The position and the size of the flow region with the vortical motion is defined by cavity parameters. The outer boundary of the vortex in the radial direction is practically coincident with the obstacle boundary. In the direction normal to the obstacle the size and the position of the region with the vortical motion largely depends on the depth parameter Δ/D_c. In the case of $\Delta/D_c = 0.5$ the center of the vortex lies inside the cavity, whereas in the case of $\Delta/D_c = 0.26$ this center is situated roughly halfway between the nozzle and the obstacle.

Fig. 4 shows the distribution of longitudinal velocity in various sections between the nozzle and the obstacle (Fig. 4a) and at various depth of a cavity (Fig. 4b). In the peripheral region of cavity

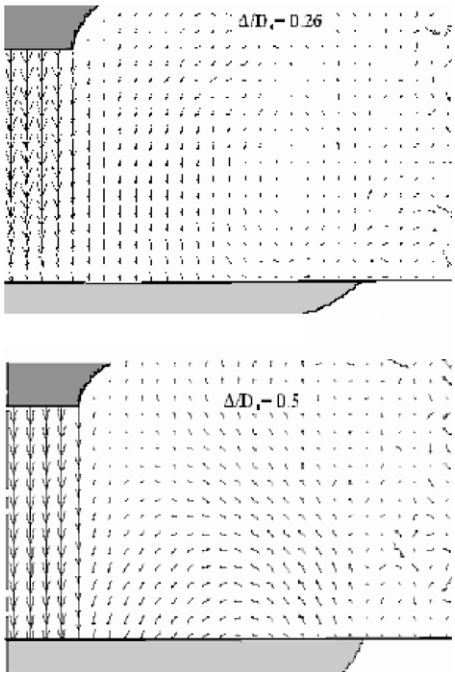

Fig. 3. The time-average flow pattern between the nozzle and the obstacle. $Re = 1.2 \times 10^4$, $S/d_0 = 2$.

there forms a reverse flow, whose boundary in the case of hemispherical cavity practically coincides with the cavity border. In the case of a shallower cavity, $\Delta/D_c = 0.26$ (see Fig. 4b), the reverse-flow region expands to periphery of a cavity due to increased mating angle at the junction between the cavity contour and the flat surface.

The maximal and minimal values of the radial flow-velocity component, whose distributions are shown in Fig. 5, fall into the region $2r/D_c \sim 0.5$–0.8, where, according to Fig. 3, the axis of the toroidal vortex is situated. In this zone, the streamwise flow velocity is close in value to the radial flow velocity, thus confirming the three-dimensional structure of the vortical motion of the medium in this region.

Thus, under certain conditions, in investigated range of parameters at $Re = 1.2 \times 10^4$ and 2.8×10^4, $S/d_0 = 2$–4, $\Delta/D_c \geqslant 0.26$, above the dimple the large-scale, toroidal vortex is formed. Besides this vortex has unstable and pulsatory character. The found out qualitative changes of flow represents the larger importance as can affect essentially on heat transfer.

3.3. Surface pressure distributions

The radial distributions of pressure coefficients are shown in Fig. 6. It is visible, that they have complex nonmonotonic character,

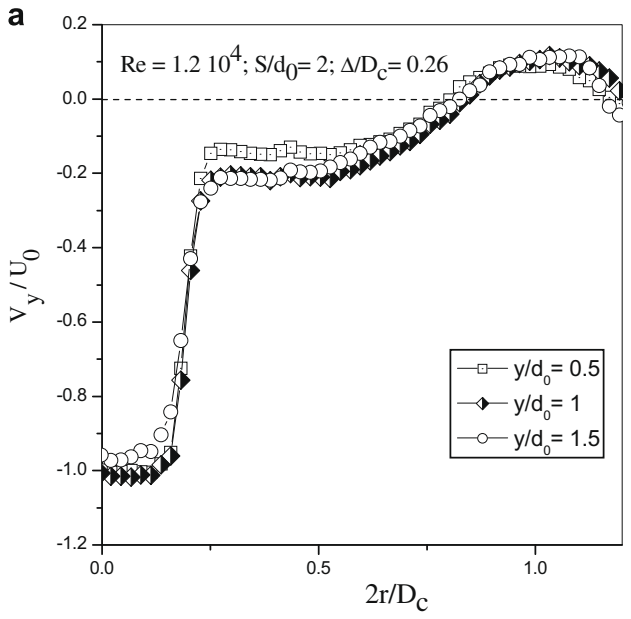

Fig. 4. Distributions of the *y*-component of flow velocity at various stations *y*/*S* between the nozzle and the cavity (a) and in different cavities (b).

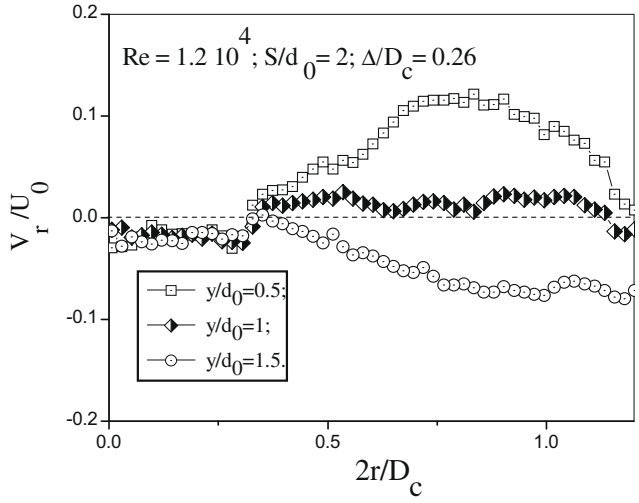

Fig. 5. Profiles of radial velocity at various stations between the nozzle and the obstacle.

depend on depth of a cavity (Δ/D_c) and from distance between nozzle and an obstacle (S/d_0). The analysis data on Fig. 6 shows, that in comparison with a flat plate at a flow of a cavity depth $\Delta/D_c = 0.12$ (Fig. 6b) the region of accelerated flow extends, reaches the cavity border, $2r/D_c = 1$.

In the hemispherical cavity ($\Delta/D_c = 0.5$, Fig. 6c) the area of acceleration also extends, but up to smaller values in a radial direction, $2r/D_c \cong 0.75$. The distributions of pressure coefficients in the vicinity of the stagnation point shaped as domes; these distributions are, however, more filled compared to the case of flat obstacle. On periphery of a cavity there is an area of negative values of pressure coefficient, area of rarefaction. It occupies approximately in a quarter of radius of a cavity. The pressure recovers to the atmospheric value, making the flow detach from the surface. The described character of distribution of pressure takes place at all distances between nozzle and obstacle, but is more strongly pronounced in conditions when the obstacle is located on an initial region of a jet. The pressure data measurements show the good correlation with results PIV-measurements, which have shown formation in dimples by depth of $\Delta/D_c = 0.26$ and 0.5 ring, toroidal vortex.

In the investigated range of Reynolds numbers distributions of pressure have a self-similarity character. It follows from Fig. 6d, where profiles of pressure at a variation of Reynolds number practically coincide among themselves.

According to modern concepts [14,15], an important role in the development of subsonic turbulent jet flows is played by regular periodic structures formed in the mixing layer of these flows and leading to periodic variations of local pressure and flow-velocity values near approached obstacles. In our experiments pressure pulsations were registered both at the flat surface and in cavities. These pulsations were low-frequency (≈1 Hz) ones, emerging at certain values of *Re* and S/d_0 (these values were different for on the flat obstacle and in cavities) in a close vicinity of the stagnation point, $\approx(1–2)d_0$. The pulsation intensity was not high (some fraction of percent of the pressure measured); nonetheless, as compared to the flat wall, this intensity in a cavity was 1.5 to 3 times higher.

3.4. Heat transfer

Investigations of heat transfer are carried out at a variation of parameters of depth of a cavity (Δ/D_c), distances between a nozzle and a barrier (S/d_0), Reynolds's numbers.

A comparison between the radial distributions of the local heat-transfer coefficients on the flat obstacle and in cavities with depths $\Delta/D_c = 0.26$ and 0.5 at fixed values S/d_0 and *Re*, is given in Fig. 7a. It is seen that the intensity of local heat transfer from the curvilinear obstacles is roughly twice lower than that from the flat obstacle. Outside the cavity the rate of heat transfer is almost zero under all examined flow conditions (Fig. 7a–d). The distance between nozzle and an obstacle as it is visible from Fig. 7b, poorly affects intensity of heat transfer.

Data obtained correspond to the above-described results of dynamic experiments, demonstrating that a global vortex is formed in the cavity, and this vortex brings back the liquid, heated in the cavity, and reduces heat transfer. At the periphery of this cavity the flow detaches from the wall, and there is no heat transfer.

The obtained arrays of instantaneous heat fluxes were used to study the heat-flow pulsations.

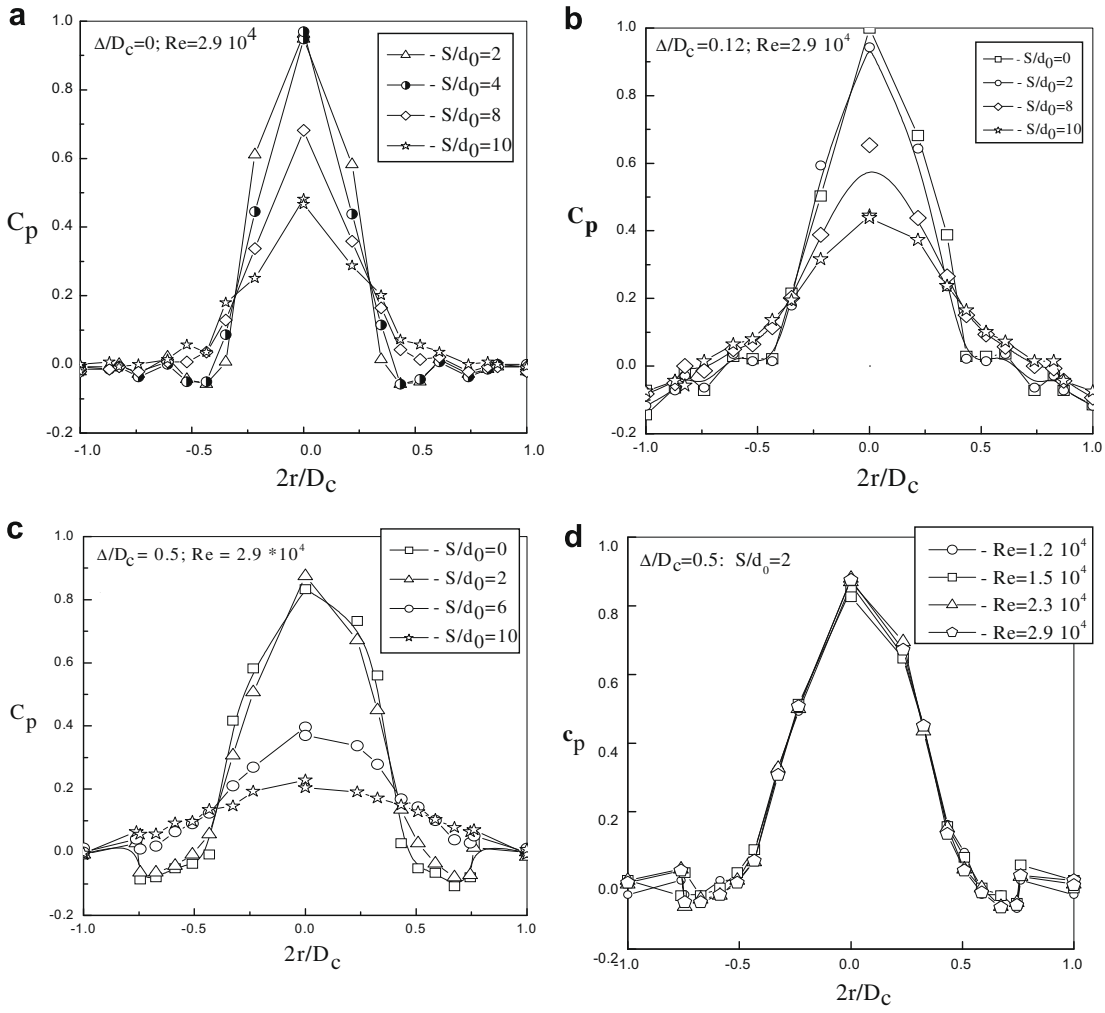

Fig. 6. Radial distributions of pressure coefficients on the obstacle.

A comparison between the time sweeps of sensor signals for the flat obstacle, and also the time sweeps of signals from sensors installed inside and outside a cavity is shown in Fig. 8. The measured data are normalized to the stagnation point heat flux q_0.

It is seen from Fig. 8 that in the vicinity of the stagnation point (r = 2.5 mm) almost no heat-flow pulsations are observed on the flat surface, showing the flow to be laminar in this region.

The signal from the sensor installed outside the cavity (r = 33 mm) has a fundamentally different waveform. The signal seems to be modulated with low-frequency oscillations. The emergence of new large-scale heat-flow pulsations well correlates with PIV data showing that in the annular air flow leaving the cavity around the peripheral regions there develops a secondary flow instability. A lower general level of the signal in this region points to reduced heat transfer outside the cavity.

Inside the cavity the heat-flow pulsations are increased that is caused by presence in dimple Taylor–Görtler vortices and a toroidal vortex in a peripheral zone of a cavity.

As could be expected, the heat-transfer intensity in the cavity decreases with increasing nozzle-to-obstacle distance, (Fig. 7b).

The heat-transfer intensity at the stagnation point as dependent on the obstacle geometry and flow Reynolds number is illustrated by Fig. 9.

The test data for the flat surface fairly well coincident with the similar data of [32,33], obey the empirical formula

$$Nu_0 = 1.24 \cdot Pr^{0.33} \cdot Re^{0.5} \cdot (S/d_0)^{-0.11}.$$

Data obtained for studied cavities lie well below the values on the flat wall, although in the hemispherical cavity up to $Re = 3 \times 10^4$ the correlation dependence $Nu_0 \approx Re$ (generalized straight line (1)) slopes at the same angle (n = 0.5), pointing to similarity of heat-transfer mechanisms at the critical point on the flat surface and in the cavity. At Re numbers above $Re = 3 \times 10^4$, dependence $Nu_0 \approx Re^n$ changes significantly.

Our experimental data on heat transfer at the stagnation point of the hemispherical cavity are compared on Fig. 9 to results of similar experiments of [27,28]. Submitted on Fig. 9 results are received at significantly differing ratios of diameters of a cavity and nozzle (parameter D_c/d_0), therefore their comparison allows to reveal influence of this factor.

The data of [28] are shown in Fig. 9 with lines 2 and 3 respectively, for two extreme values of the diameter ratio, $D_c/d_0 = 44$ and 16. With a small-diameter nozzle, $D_c/d_0 = 44$, the rate of heat transfer at the stagnation point exceeds the value on the flat surface, and the power exponent at the Reynolds number in the law of heat transfer also assumed an increased value

$$Nu_0 = 0.798 \cdot Re^{0.604} \cdot Pr^{0.4} \cdot (S/d_0)^{-0.22}.$$

On the decrease of the value of D_c/d_0 to 16 the experimental dependence of Nu versus Re decreases to approach the present experimental data for $D_c/d_0 = 5.4$, the heat-transfer intensity reaching values lower than on the flat obstacle.

The measurement data of [27] are shown in Fig. 9 with lines 4 and 5, respectively, to $D_c/d_0 = 11.2$ and 29.4. According to the data

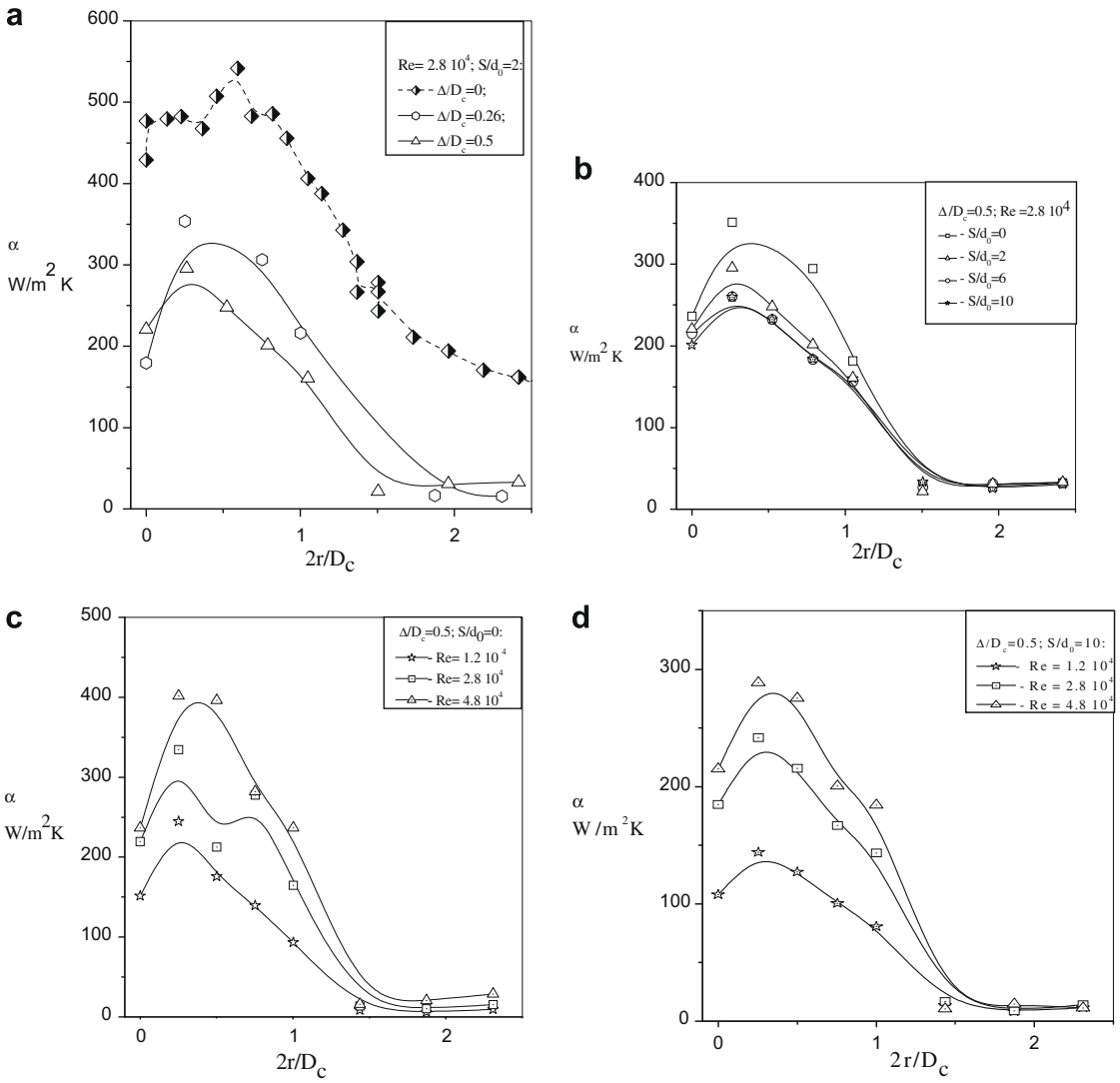

Fig. 7. Local heat-transfer coefficients at a variation of parameters of a flow and a cavity.

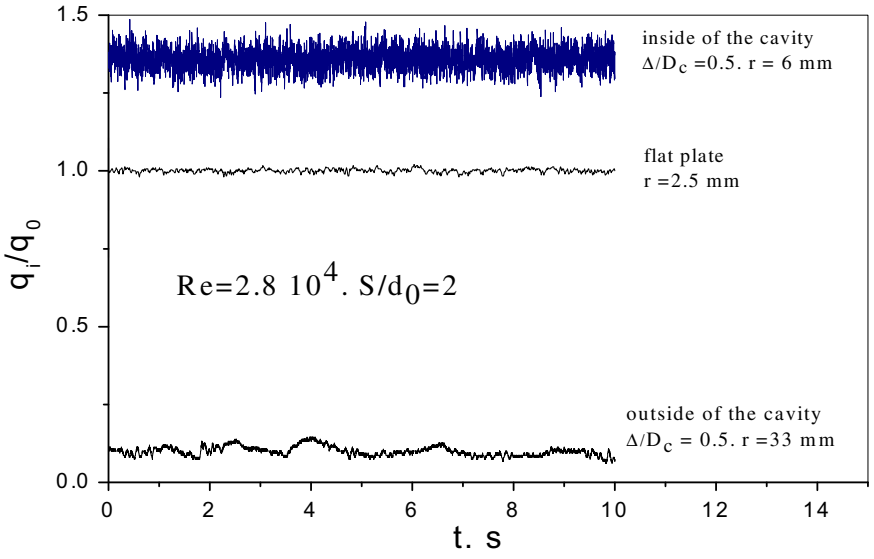

Fig. 8. Comparison between the time sweeps of instantaneous heat fluxes.

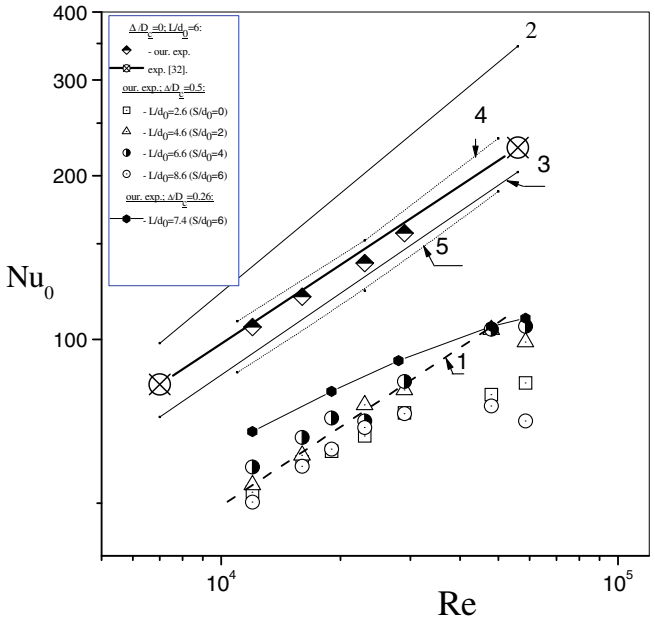

Fig. 9. Heat transfer at the stagnation point on the flat obstacle and in cavities. 1 – our data in cavity; 2, 3 – exp. [28] $L/d_0 = 6$, $\Delta/D_c = 0.5$; 2 – $D_c/d_0 = 44$, 3 – 16. 4, 5 – exp. [27] $L/d_0 = 6$, $\Delta/D_c = 0.5$; 4 – $D_c/d_0 = 11.2$, 5 – $D_c/d_0 = 29.4$.

obtained in [27], the rate of heat transfer at the stagnation point decreases with increasing parameter D_c/d_0. This result contradicting to the data [28] and being in rather poor agreement with the present data.

Data of primary significance for industrial applications are data concerning the mean heat transfer from the entire cavity surface streamlined with the impinging jet flow. The mean heat-transfer coefficient in the hemispherical cavity ($\Delta/D_к = 0.5$) was found by integrating the radial distributions over the entire cavity surface on the assumption that the distributions were axisymmetric. The experimental mean Nusselt versus Reynolds number are shown in Fig. 10. In the interval of nozzle-to-obstacle distances $S/d_0 = 0$–4 the experimental data are coincident. As we move farther from the obstacle, the mean rate of heat transfer from the cavity starts decreasing. Line 1, approximating the experimental data for $S/d_0 = 0$–4 within the range of Re numbers of 10^4–6×10^4, takes the form

$$Nu_m = \alpha_m \cdot d_0/\lambda = 0.37 Re^{0.5}. \quad (1)$$

As we can see, despite intensive turbulent pulsations of the heat flux, registered by the probes – Fig. 8 – correlation dependence (*1*) refers to a laminar law of heat transfer with power exponent $n = 0.5$. This contradiction again points the fact that the heat-transfer mechanism under the considered conditions is essentially connected with formation of a global vortex, which returns the heated flow back and, hence, reduces heat transfer.

For comparison, line 2 in Fig. 10 shows the empirical dependence borrowed from [34], which describes the mean heat transfer on the flat surface approached by a circular jet with $S/d_0 = 4$. The diameter of the surface over which the averaging was performed equaled the cavity diameter in our experiments, $D_c = 46$ mm. The rate of heat transfer on the flat surface is 1.6 to 2 times greater than that in the cavity. Yet, considering the twice greater total surface area of the hemispherical cavity, for the integral heat flux at high Reynolds numbers we obtain the same value as on the flat surface. The integral heat flux from the hemispherical cavity in the interval flow Reynolds numbers $Re < 3 \times 10^4$ being more intense, as on the flat surface.

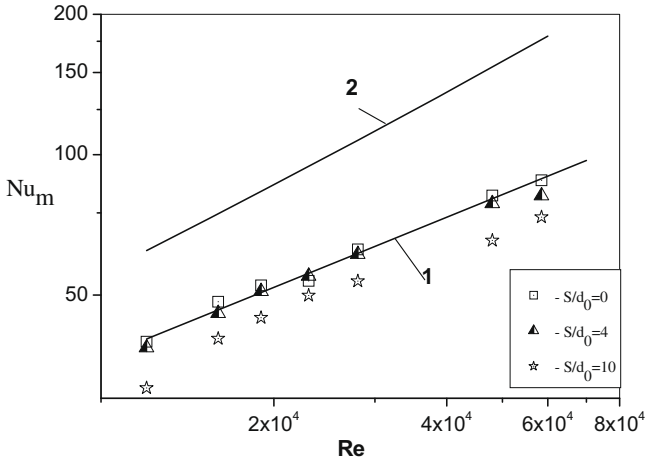

Fig. 10. The mean Nusselt number versus Reynolds number for a spherical cavity. Lines 1 and 2 – empirical relations for a cavity (formula (1)) and for a flat surface [34].

4. Conclusions

1. An experimental study of flow characteristics and heat transfer characteristics for the round jet flowing around the obstacle in the form of single spherical cavity $Re = (1.2–5.8) \times 10^4$, $D_c/d_0 = 5.2$, $S/d_0 = 0–10$, $\Delta/D_c = 0–0.5$ has been presented.
2. At $\Delta/D_c \leqslant 0.13$ flow of a dimple qualitatively coincides with a flow of a flat plate. Cavities with depth $\Delta/D_c \geqslant 0.26$ generate a large-scale pulsing toroidal vortex. This vortex results in formation of returnable flow of the gas heated up in a cavity and decrease in heat exchange. The local heat-transfer intensity in the hemispherical cavity is lower than that on a flat obstacle; yet, this reduction is almost fully compensated by increased area of the heat-exchanging surface. Outside the cavity with the depth $\Delta/D_c \geqslant 0.26$ the air flow does not join the obstacle surface and the heat transfer is practically absent in this zone.
3. The heat transfer in a hemispherical cavity largely depends on the ratio between the cavity and nozzle diameters (параметра D_c/d_0) and in comparison with a flat obstacle can both to grow, and to decrease. The problem of influence of the specified geometrical factor by present time remains open and demands the further investigations.
4. It should be noted that in the majority of studies the specific features of heat-transfer processes proceeding during jet impingement cooling of curvilinear obstacles were believed to result from Taylor–Gőrtler vortices formed near the obstacle surface. Our experiments showed that under certain conditions in the flow impinging on a hemispherical cavity, along with the formation of near-surface Taylor–Gőrtler vortices there occurs large-scale restructuring of the whole flow field. According to our research, the whole flow field and heat-transfer mechanism change significantly in addition to formation of the near-surface Taylor–Gőrtler vortices at the flow around a semispherical cavity.

Acknowledgement

This work was supported by the Russian Foundation for Basic Research (Grant No. 07-08-00025).

References

[1] B.N. Yudaev, M.S. Mikhailov, V.K. Savin, Heat Transfer in Jet Flows Impinging on Obstacles, Mashinostroenie, Moscow, 1977 (in Russian).

[2] H. Martin, Heat and mass transfer between impinging gas jet and solid surface, Advances in Heat Transfer, vol. 13, Academic Press, New York, 1977.
[3] E.P. Dyban, A.I. Mazur, Convective Heat Transfer in Jet Flows Impinging on Bodies, Naukova Dumka, Kiev, 1982 (in Russian).
[4] E.P. Dyban, A.I. Mazur, E.Ya. Epik, Flat air jet outflow into a blind pass, J. Eng. Phys. 20 (6) (1971) 1020–1026.
[5] V.I. Terekhov, S.V. Kalinina, Flow and heat transfer in a single spherical cavity state of the problem and unanswered questions. (Review), Thermophys. Aeromech. 9 (4) (2002) 497–520.
[6] V.N. Afanasyev, Y.P. Chudnovsky, A.I. Leontiev, P.S. Roganov, Turbulent flow friction and heat transfer characteristics for spherical cavities on a flat plate, Exp. Thermal Fluid Sci. 7 (1993) 1–8.
[7] V.I. Terekhov, S.V. Kalinina, Yu.M. Mshvidobadze, Heat-transfer coefficient and aerodynamic resistance on a surface with a single dimple, Enhanced Heat Transfer 4 (1997) 131–145.
[8] G.I. Mahmood, P.M. Ligrani, Heat transfer in a dimpled channel combined influences of aspect ratio, temperature ratio, Reynolds number, and flow structure, Int. J. Heat Mass Transfer 45 (2002) 2011–2020.
[9] K. Kanokjaruvijit, R.F. Martinez-Botas, Parametric effects on heat transfer of impingement on dimpled surface, J. Turbomashinery ASME 127 (2005) 287–296.
[10] K. Kanokjaruvijit, R.F. Martinez-Botas, Jet impingement on a dimpled surface with different crossflow schemes, Int. J. Heat Mass Transfer 48 (2005) 16–170.
[11] S.V. Ekkad, D. Kontrovitz, Jet impingement heat transfer on dimpled target surfaces, Int. J. Heat Fluid Flow 23 (2002) 22–28.
[12] G.S. Azad, Y. Huang, J.-C. Han, Impingement heat transfer on dimpled surfaces using a transient liquid crystal technique, J. Thermophys. Heat Transfer 14 (2000) 186–193.
[13] Ch.-M. Ho, N.S. Nosseir, Large coherent structures in an impinging jet, Turbulent shear flows 2, in: Papers from Second International Symposium on Turbulent Shear Flows, London, July 1979, Berlin, 1980, pp. 297–304.
[14] S.V. Alekseenko, A.V. Bilsky, O.M. Heinz, B.B. Ilyushin, D.M. Markovich, Near-wall characteristics of impinging turbulent jet, in: Proc. Fourth International Symposium on Turbulence, Heat and Mass Transfer, Antalya, Turkey, 2003, pp. 235–241.
[15] L. Tianshu, J.P. Sullivan, Heat transfer and flow structures in an excited circular impinging jet, Int. J. Heat Mass Transfer 39 (17) (1996) 3695–3706.
[16] J.C.Y. Koh, J.P. Hartnett, Measured pressure distribution and local heat transfer rates for flow over concave hemisphere, ARS J. 31 (1) (1961) 71–75.
[17] Y. Kornblum, R.J. Goldstein, Jet impingement on semicircular concave and convex surface, part one recovery factor, in: Proc. Int. Symp. Physics of Heat Transfer in Boiling and Condensation, Moscow, 1997, pp. 597–602.
[18] Y. Kornblum, R.J. Goldstein, Jet impingement on semicircular concave and convex surface, part two heat transfer, in: Proc. Int. Symp. Physics of Heat Transfer in Boiling and Condensation, Moscow, 1997, pp. 603–608.
[19] C. Cornano, A.S. Fleischer, R.J. Goldstein, Flow visualization of a round jet impinging on cylindrical surfaces, Exp. Thermal Fluid Sci. 20 (1999) 66–78.
[20] P. Hrycak, Heat transfer from a row of impinging jets to concave cylindrical surface, Int. J. Heat Mass Transfer 24 (1981) 407–419.
[21] T.L. Chan, Y. Zhou, M.H. Liu, C.W. Leung, Mean flow and turbulence measurements of the impingement wall jet on a semi-circular convex surface, Exp. Fluids 34 (2003) 140–149.
[22] Y.T. Yang, C.H. Hwang, Numerical simulations on the hydrodynamics of a turbulent slot jet impinging on a semi-cylindrical convex surface, Numer. Heat Transfer Ser. Appl. 46 (2004) 995–1008.
[23] M. Choi, H.S. Yoo, G. Yang, S.K. Lee, D.K. Sohn, Measurements of impinging jet flow and heat transfer on a semi-circular concave surface, Int. J. Heat Mass Transfer 43 (2000) 1811–1822.
[24] G. Hu, L. Zhang, Experimental and numerical study on heat transfer with impinging circular jet on a convex hemispherical surface, Heat Transfer Eng. 28 (2007) 1008–1016.
[25] D.H. Lee, Y.S. Chung, M.G. Kim, Turbulent heat transfer from a convex hemispherical surface to a round impinging jet, Int. J. Heat Mass Transfer 42 (1999) 1147–1156.
[26] D.H. Lee, Y.S. Chung, M.G. Kim, Turbulent flow and heat transfer measurements on a curved surface with a fully developed round impinging jet, Int. J. Heat Fluid Flow 18 (1997) 169.
[27] D.H. Lee, Y.S. Chung, S.Y. Won, The effect of concave surface curvature on heat transfer from a fully developed round impinging jet, Int. J. Heat Mass Transfer 42 (1999) 2489–2497.
[28] P. Hrycak, Heat transfer and flow characteristics of jets impinging on a concave hemispherical plate, in: Proc. 7th Int. Heat Trans. Conf. Munchen Hemisphere Publ. Corp., Wash., New York, London, vol. 3, 1982, pp. 357–362.
[29] V.I. Terekhov, V.L. Barsanov, S.V. Kalinina, Yu.M. Mshvodobadze, Investigation into the flow structure and heat transfer of a jet flow impinging perpendicularly on a complex-geometry obstacle, in: Proc. XXVII Siberian Thermophysical Seminar dedicated to the 90th Anniversary of S.S. Kutateladze, Moscow, Novosibirsk, October 1–5, 2004. Novosibirsk, Inst. of Thermophys., CD-publication ISBN-5-89017-027-9, 143, 2004.
[30] V.I. Terekhov, V.L. Barsanov, S.V. Kalinina, Yu.M. Mshvidobadze, Experimental study of flow structure and heat transfer under a jet flow past a spherical-cavity obstacle, J. Eng. Phys. Thermophys. 79 (4) (2006) 657–665.
[31] S.Z. Sapozhnikov, V.Yu. Mityakov, A.V. Mityakov, Gradient Heat-Flow Probes, St. Petersburg, 2003 (in Russian).
[32] R. Gardon, J. Cobonque, Heat transfer between a flat plate and jets of air impinging on it, in: Proc. Int. Heat Transfer Conference, New York, 1961, pp. 454–460.
[33] D. Lee, R. Greif, S.J. Lee, J.H. Lee, Heat transfer from a flat plate to a fully developed axisymmetric impinging jet, J. Heat Transfer 117 (1995) 772–776.
[34] E.U. Schlunder, V. Gnielinski, Warme – und stoffubertragung zwischen gut und aufprallenden Dusenstrahl, Chem. Ing. Technik. 39 (1967) 578–584.